

Salient Object Detection: A Benchmark

Ali Borji, Ming–Ming Cheng, Huaizu Jiang and Jia Li

Abstract—We extensively compare, qualitatively and quantitatively, 40 state-of-the-art models (28 salient object detection, 10 fixation prediction, 1 objectness, and 1 baseline) over 6 challenging datasets for the purpose of benchmarking salient object detection and segmentation methods. From the results obtained so far, our evaluation shows a consistent rapid progress over the last few years in terms of both accuracy and running time. The top contenders in this benchmark significantly outperform the models identified as the best in the previous benchmark conducted just two years ago. We find that the models designed specifically for salient object detection generally work better than models in closely related areas, which in turn provides a precise definition and suggests an appropriate treatment of this problem that distinguishes it from other problems. In particular, we analyze the influences of center bias and scene complexity in model performance, which, along with the hard cases for state-of-the-art models, provide useful hints towards constructing more challenging large scale datasets and better saliency models. Finally, we propose probable solutions for tackling several open problems such as evaluation scores and dataset bias, which also suggest future research directions in the rapidly-growing field of salient object detection.

Index Terms—Salient object detection, saliency, explicit saliency, visual attention, regions of interest, objectness, segmentation, interestingness, importance, eye movements

I. INTRODUCTION

VISUAL attention, the astonishing capability of human visual system to selectively process only the *salient* visual stimuli in details, has been investigated by multiple disciplines such as cognitive psychology, neuroscience, and computer vision [2]–[5]. Following cognitive theories (e.g., *feature integration theory (FIT)* [6], *guided search model* [7], [8]) and early attention models (e.g., Koch and Ullman [9] and Itti *et al.* [10]), hundreds of computational saliency models have been proposed to detect salient visual subsets from images and videos.

Despite the psychological and neurobiological definitions, the concept of visual saliency is becoming vague in the field of computer vision. Some visual saliency models (e.g., [3], [10]–[16]) aimed to *predict human fixations* as a way to test their accuracy in saliency detection, while other

models [17]–[19], which were often driven by computer vision applications such as content-aware image resizing and photo visualization [20], attempted to *identify salient regions/objects* and used explicit saliency judgments for evaluation [21]. Although both types of saliency models are expected to be applicable interchangeably, their generated saliency maps actually demonstrate remarkably different characteristics due to the distinct purposes in saliency detection. For example, fixation prediction models usually pop-out sparse blob-like salient regions, while salient object detection models often generate smooth connected areas. On the one hand, detecting large salient areas often causes severe false positives for fixation prediction. On the other hand, popping-out only sparse salient regions causes massive misses in detecting salient regions and objects.

To separate these two types of saliency models, in this study we provide a precise definition and suggest an appropriate treatment of salient object detection. Generally, a salient object detection model should, *first* detect the salient attention-grabbing objects in a scene, and *second*, segment the entire objects. Usually, the output of the model is a saliency map where the intensity of each pixel represents its probability of belonging to salient objects. From this definition, we can see that this problem in its essence is a figure/ground segmentation problem, and the goal is to only segment the salient foreground object from the background. Note that it slightly differs from the traditional image segmentation problem that aims to partition an image into perceptually coherent regions.

The value of salient object detection models lies on their applications in many areas such as computer vision, graphics, and robotics. For instance, these models have been successfully applied in many applications such as object detection and recognition [22]–[29], image and video compression [30], [31], video summarization [32]–[34], photo collage/media re-targeting/cropping/thumb-nailing [20], [35], [36], image quality assessment [37]–[39], image segmentation [40]–[43], content-based image retrieval and image collection browsing [44]–[47], image editing and manipulating [48]–[51], visual tracking [52]–[58], object discovery [59], [60], and human-robot interaction [61], [62]. The field of salient object detection develops very fast. Many new models and benchmark datasets have been proposed since our earlier benchmark conducted two years ago [1]. Yet, it is unclear how the new algorithms fare against previous models and new datasets. Are there any *real improvements* in this field or we are just fitting models to datasets? It is also interesting to test the performance of old high-performing models on the new benchmark datasets. A recent exhaustive review of salient object detection models can be found in [28].

A. Borji is with the Computer Science Department, University of Wisconsin, Milwaukee, WI 53211. E-mail: borji@uwm.edu

M.M Cheng is with the Department of Engineering Science, University of Oxford, Parks Road, Oxford OX1 3PJ. E-mail: cmm.thu@gmail.com

H. Jiang is with the Institute of Artificial Intelligence and Robotics, Xi'an Jiaotong University, China. E-mail: hzjiang@mail.xjtu.edu.cn

J. Li is with State Key Laboratory of Virtual Reality Technology and Systems, School of Computer Science and Engineering, Beihang University. He is also with the International Research Institute for Multidisciplinary Science (IRIMS) at Beihang University, Beijing, China. E-mail: jiali@buaa.edu.cn

An earlier version of this work has been published in ECCV 2012 [1].

First two authors contributed equally.

Manuscript received xx 2014.

In this study, we compare and analyze models from three categories: 1) salient object detection, 2) fixation prediction, and 3) object proposal generation¹. The reason to include the latter two types of models is to conduct across-category comparison and to study whether models specifically designed for salient object detection show actual advantage over models for fixation prediction and object proposal generation. This is particularly important since these models have different objectives and generate visually distinctive maps. We also include a baseline model to study the effect of center bias in model comparison. In summary, we hope that such a benchmark not only allows researchers to compare their models with other algorithms but also helps identify the chief factors affecting the performance of salient object detection models.

II. SALIENT OBJECT DETECTION BENCHMARK

In this benchmarking, we focus on evaluating models whose input is a single image. This is due to the fact that salient object detection on a single input image is the main research direction, while the comprehensive evaluation of models working on multiple input images (*e.g.*, co-salient object detection) lacks public benchmark datasets.

A. Compared Models

In this study, we run 40 models in total (28 salient object detection models, 10 fixation prediction models, 1 objectness proposal model, and 1 baseline) whose codes or executables were accessible (see Fig. 1 for a complete list). The baseline model, denoted as ‘‘Average Annotation Map (AAM),’’ is simply the average of ground-truth annotations of all images on each dataset. Note that AAM often has a larger activation at the image center (see Fig. 2), and we can thus study the effect of center bias in model comparison.

B. Datasets

Since there exist many datasets that differ in number of images, number of objects per image, image resolution and annotation form (bounding box or accurate region mask), it is likely that models may rank differently across datasets. Hence, to come up with a fair comparison, it is necessary to run models over multiple datasets so as to draw objective conclusions. A good model should perform well over almost all datasets. Toward this end, six datasets were chosen for model comparison, including: 1) **MSRA10K** [98], 2) **ECSSD** [75], 3) **THUR15K** [98], 4) **JuddDB** [99], 5) **DUT-OMRON** [76], and 6) **SED2** [1], [100]. These datasets were selected based on the following four criteria: 1) being widely-used, 2) containing a large number of images, 3) having different biases (*e.g.*, number of salient objects, image clutter, center-bias), and 4) potential to be used as benchmarks in the future research.

MSRA10K is a descendant of the MSRA dataset [17]. It contains 10,000 annotated images that covers all the 1,000

¹Object proposal generation is a recently emerging trend which attempts to detect image regions that may contain objects from any object category (*i.e.*, category independent object proposals).

#	Model	Pub	Year	Code	Time(s)	Cat.
1	LC [63]	MM	2006	C	.009	Salient Object Detection
2	AC [64]	ICVS	2008	C	.129	
3	FT [18]	CVPR	2009	C	.072	
4	CA [65]	CVPR	2010	M + C	40.9	
5	MSS [66]	ICIP	2010	C	.076	
6	SEG [67]	ECCV	2010	M + C	10.9	
7	RC [68]	CVPR	2011	C	.136	
8	HC [68]	CVPR	2011	C	.017	
9	SWD [69]	CVPR	2011	M + C	.190	
10	SVO [70]	ICCV	2011	M + C	56.5	
11	CB [71]	BMVC	2011	M + C	2.24	
12	FES [72]	Img.Anal.	2011	M + C	.096	
13	SF [73]	CVPR	2012	C	.202	
14	LMLC [74]	TIP	2013	M + C	140.	
15	HS [75]	CVPR	2013	EXE	.528	
16	GMR [76]	CVPR	2013	M	.149	
17	DRFI [77]	CVPR	2013	C	.697	
18	PCA [78]	CVPR	2013	M + C	4.34	
19	LBI [79]	CVPR	2013	M + C	251.	
20	GC [80]	ICCV	2013	C	.037	
21	CHM [81]	ICCV	2013	M + C	15.4	
22	DSR [82]	ICCV	2013	M + C	10.2	
23	MC [83]	ICCV	2013	M + C	.195	
24	UFO [84]	ICCV	2013	M + C	20.3	
25	MNP [50]	Vis.Comp.	2013	M + C	21.0	
26	GR [85]	SPL	2013	M + C	1.35	
27	RBD [86]	CVPR	2014	M	.269	
28	HDCT [87]	CVPR	2014	M	4.12	
1	IT [10]	PAMI	1998	M	.302	Fixation Prediction
2	AIM [88]	JOV	2006	M	8.66	
3	GB [89]	NIPS	2007	M + C	.735	
4	SR [90]	CVPR	2007	M	.040	
5	SUN [91]	JOV	2008	M	3.56	
6	SeR [92]	JOV	2009	M	1.31	
7	SIM [93]	CVPR	2011	M	1.11	
8	SS [94]	PAMI	2012	M	.053	
9	COV [95]	JOV	2013	M	25.4	
10	BMS [96]	ICCV	2013	M + C	.575	
1	OBJ [97]	CVPR	2010	M+C	3.01	-
1	AAM	-	-	-	-	-

Fig. 1. Compared salient object detection, fixation prediction, object proposal generation, and baseline models sorted by their publication year {M= Matlab, C= C/C++, EXE = executable}. The average running time is tested on MSRA10K dataset (typical image resolution 400×300) using a desktop machine with Xeon E5645 2.4 GHz CPU and 8GB RAM. We evaluate those models whose codes or executables are available.

images in the popular ASD dataset [18]. **THUR15K** and **DUT-OMRON** are used to compare models on a large scale. **ECSSD** contains a large number of semantically meaningful but structurally complex natural images. The reason to include **JuddDB** was to assess performance of models over scenes with multiple objects with high background clutter. Finally, we also evaluate models over **SED2** to check whether salient object detection algorithms can perform well on images containing more than one salient object (*i.e.*, two in **SED2**). Fig. 2 shows the AAM model output of six benchmark datasets to illustrate their different center biases. See Fig. 3 for representative images and annotations from each dataset.

We illustrate in Fig. 4 the statistics of the six chosen datasets. In Fig. 4(a), we show the normalized distances from the centroid of salient objects to the corresponding image centers. We can see that salient objects in **ECSSD** have the shortest distance to image centers, while salient objects in **SED2** have the longest distances. This is reasonable since

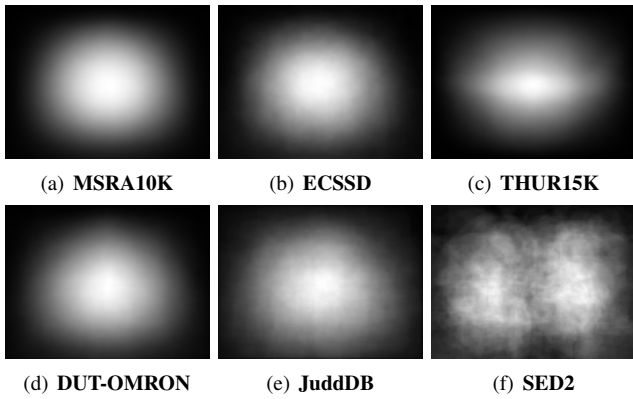


Fig. 2. Average annotation maps of six datasets used in benchmarking.

images in **SED2** usually have two objects aligned around opposite image borders. Moreover, we can see that the spatial distribution of salient objects in **JuddDB** has a larger variety than other datasets, indicating that this dataset have smaller positional bias (*i.e.*, center-bias of salient objects and border-bias of background regions).

In Fig. 4(b), we aim to show the complexity of images in six benchmark datasets. Toward this end, we apply the segmentation algorithm by Felzenszwalb *et al.* [101] to see how many super-pixels (*i.e.*, homogeneous regions) can be obtained on average from salient objects and background regions of each image, respectively. In this manner, we can use this measure to reflect how challenging a benchmark is since massive super-pixels often indicate complex foreground objects and cluttered background. From Fig. 4(c), we can see that **JuddDB** is the most challenging benchmark since it has an average number of 493 super-pixels from the background of each image. On the contrary, **SED2** contains fewer number of super-pixels in foreground and background regions, indicating that images in this benchmark often contain uniform regions and are easy to process.

In Fig. 4(c), we demonstrate the average object sizes of these benchmarks, while the size of each object is normalized by the size of the corresponding image. We can see that **MSRA10K** and **ECSSD** datasets have larger objects while **SED2** has smaller ones. In particular, we can see that some benchmarks contain a limited number of image regions with large foreground objects. By jointly considering the center-bias property, it becomes very easy to achieve a high precision on these images.

C. Evaluation Measures

There are several ways to measure the agreement between model predictions and human annotations [21]. Some metrics evaluate the overlap between a tagged region while others try to assess the accuracy of drawn shapes with object boundary. In addition, some metrics have tried to consider both boundary and shape [102].

Here, we use three universally-agreed, standard, and easy-to-understand measures for evaluating a salient object detection model. The first two evaluation metrics are based on the overlapping area between subjective annotation and

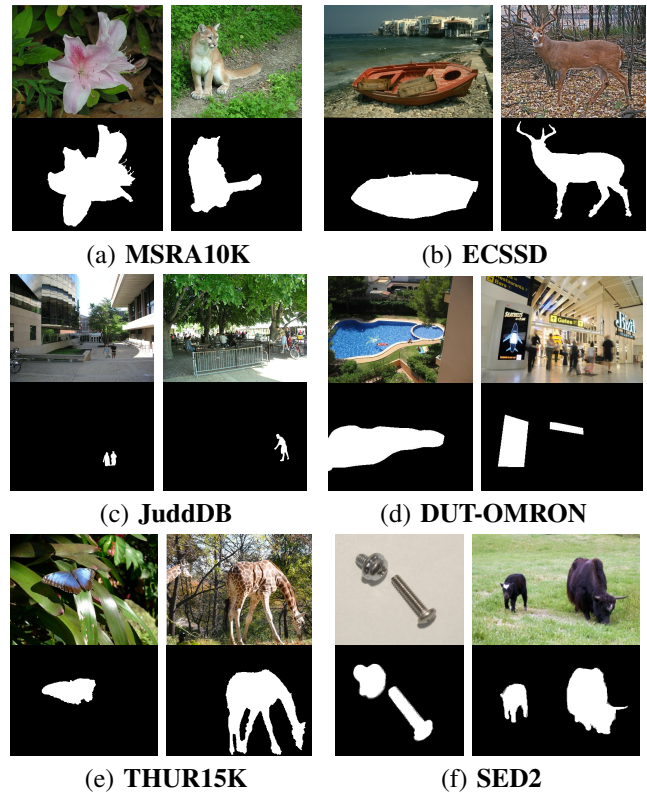


Fig. 3. Images and pixel-level annotations from six salient object datasets.

saliency prediction, including the precision-recall (PR) and the receiver operating characteristics (ROC). From these two metrics, we also report the F-Measure, which jointly considers recall and precision, and AUC, which is the area under the ROC curve. Moreover, we also use the third measure which directly computes the mean absolute error (MAE) between the estimated saliency map and ground-truth annotation. For the sake of simplification, we use S to represent the predicted saliency map normalized to $[0, 255]$ and G to represent the ground-truth binary mask of salient objects. For a binary mask, we use $|\cdot|$ to represent the number of non-zero entries in the mask.

Precision-recall (PR). For a saliency map S , we can convert it to a binary mask M and compute *Precision* and *Recall* by comparing M with ground-truth G :

$$Precision = \frac{|M \cap G|}{|M|}, \quad Recall = \frac{|M \cap G|}{|G|} \quad (1)$$

From this definition, we can see that the binarization of S is the key step in the evaluation. Usually, there are three popular ways to perform the binarization. In the first solution, Achanta *et al.* [18] proposed the image-dependent adaptive threshold for binarizing S , which is computed as twice as the mean saliency of S :

$$T_a = \frac{2}{W \times H} \sum_{x=1}^W \sum_{y=1}^H S(x, y), \quad (2)$$

where W and H are the width and the height of the saliency map S , respectively.

The second way to bipartite S is to use a fixed threshold which changes from 0 to 255. On each threshold, a pair

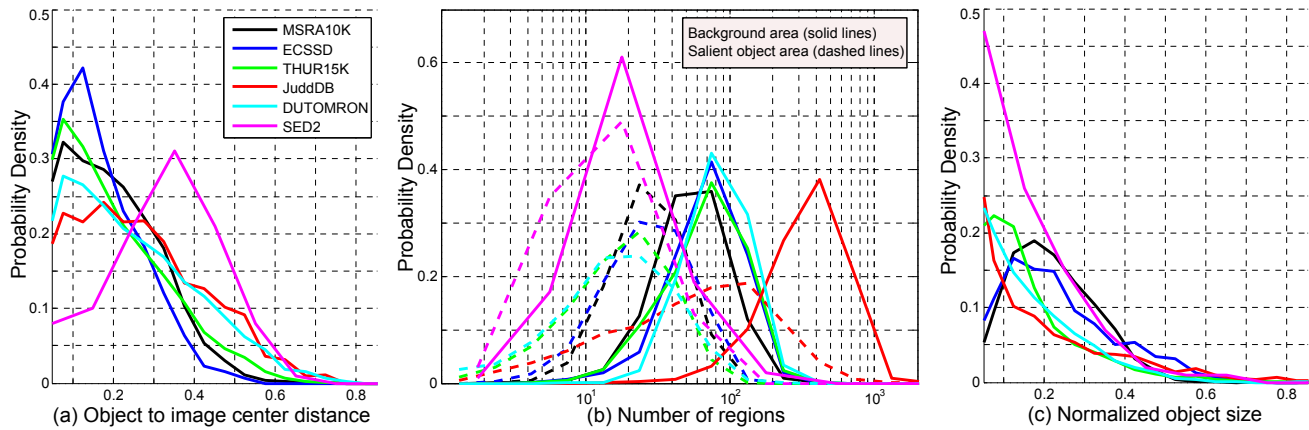


Fig. 4. Statistics of the benchmark datasets. a) distribution of normalized object distance from image center, b) distribution of super-pixel number on salient objects and image background, and c) distribution of normalized object size.

of precision/recall scores are computed, and are finally combined to form a precision-recall (PR) curve to describe the model performance at different situations.

The third way of binarization is to use the SaliencyCut algorithm [68]. In this solution, a loose threshold, which typically results in good recall but relatively poor precision, is used to generate the initial binary mask. Then the method iteratively uses the GrabCut segmentation method [103] to gradually refine the binary mask. The final binary mask is used to re-compute the precision-recall value.

F-measure. Usually, neither *Precision* nor *Recall* can comprehensively evaluate the quality of a saliency map. To this end, the F-measure is proposed as a weighted harmonic mean of them with a non-negative weight β :

$$F_{\beta} = \frac{(1 + \beta^2) Precision \times Recall}{\beta^2 Precision + Recall}. \quad (3)$$

As suggested by many salient object detection works (e.g., [18], [68], [73]), β^2 is set to 0.3 to raise more importance to the *Precision* value. The reason for weighting precision more than recall is that recall rate is not as important as precision (see also [104]). For instance, 100% recall can be easily achieved by setting the whole region to foreground.

According to the different ways for saliency map binarization, there exist two ways to compute F-Measure. When the adaptive threshold or GrabCut algorithm is used for the binarization, we can generate a single F_{β} for each image and the final F-Measure is computed as the average F_{β} . When using fixed thresholding, the resulted PR curve can be scored by its maximal F_{β} , which is a good summary of the detection performance (as suggested in [105]). As defined in (3), F-Measure is the weighted harmonic mean of precision and recall, thus share the same value bounds as precision and recall values, i.e. [0, 1].

Receiver operating characteristics (ROC) curve. In addition to the *Precision*, *Recall* and F_{β} , we can also report the false positive rate (*FPR*) and true positive rate (*TPR*) when binarizing the saliency map with a set of fixed

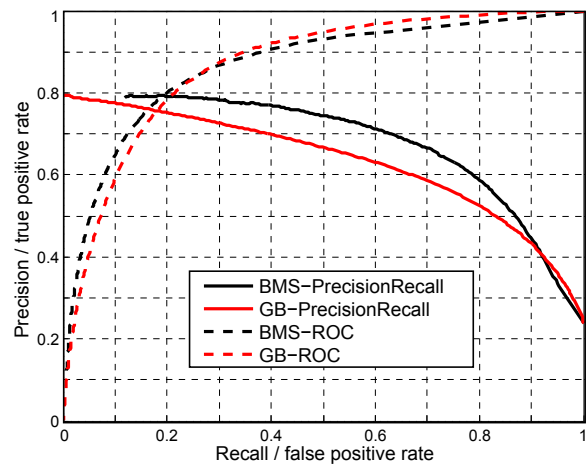


Fig. 5. PR and ROC curves for BMS [96] and GB [89] over ECSSD.

thresholds:

$$TPR = \frac{|M \cap G|}{|G|}, \quad FPR = \frac{|M \cap \bar{G}|}{|\bar{G}|} \quad (4)$$

where \bar{M} and \bar{G} denote the opposite of the binary mask M and ground-truth, respectively. The ROC curve is the plot of *TPR* versus *FPR* by varying the threshold T_f .

Area under ROC curve (AUC) score. While ROC is a two-dimensional representation of a model's performance, the AUC distills this information into a single scalar. As the name implies, it is calculated as the area under the ROC curve. A perfect model will score an AUC of 1, while random guessing will score an AUC around 0.5.

Mean absolute error (MAE) score. The overlap-based evaluation measures introduced above do not consider the true negative saliency assignments, i.e., the pixels correctly marked as non-salient. This favors methods that successfully assign saliency to salient pixels but fail to detect non-salient regions over methods that successfully detect non-salient pixels but make mistakes in determining the salient ones [73], [80]. Moreover, in some application scenarios [106] the quality of the weighted, continuous saliency maps may be of higher importance than the binary

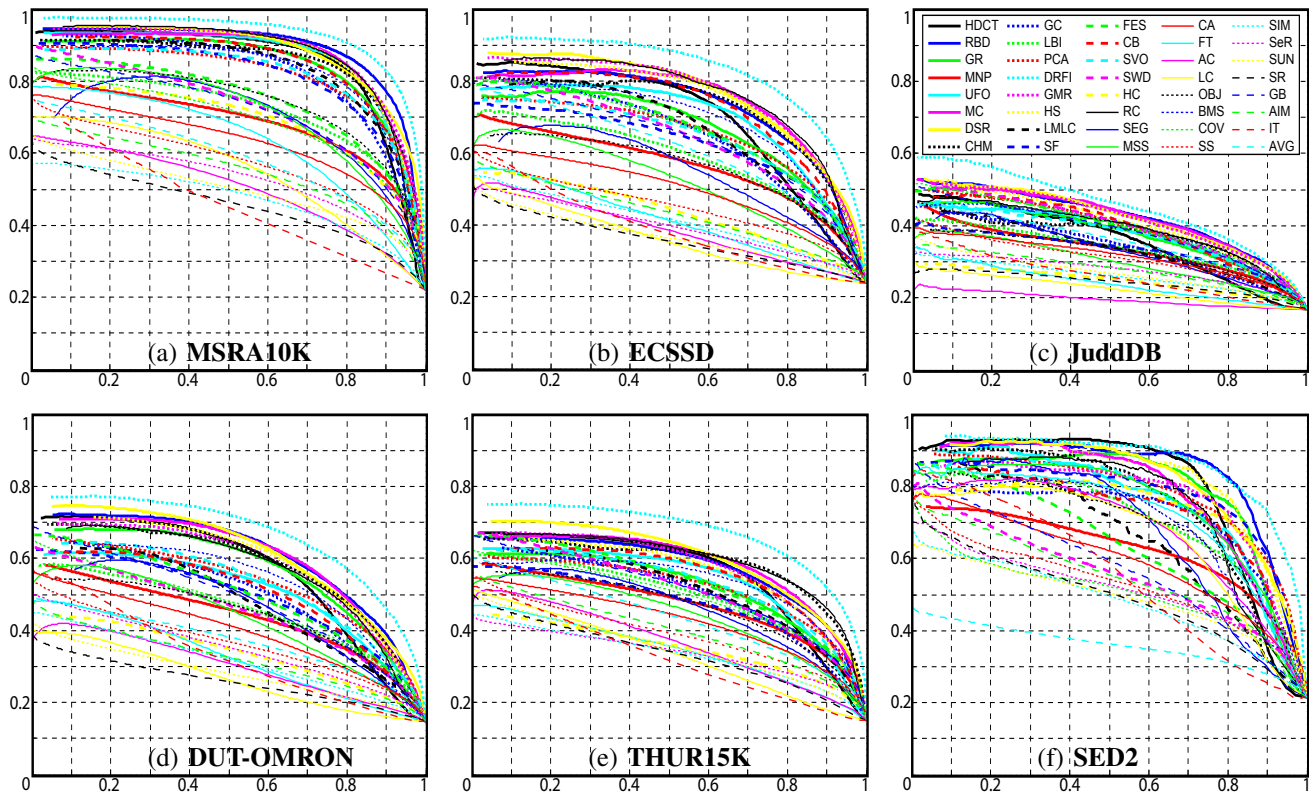


Fig. 6. Precision (vertical axis) and recall (horizontal axis) curves of saliency methods on 6 popular benchmark datasets.

masks. For a more comprehensive comparison we therefore also evaluate the mean absolute error (MAE) between the continuous saliency map \bar{S} and the binary ground truth \bar{G} , both normalized in the range $[0, 1]$. The MAE score is defined as:

$$MAE = \frac{1}{W \times H} \sum_{x=1}^W \sum_{y=1}^H |\bar{S}(x, y) - \bar{G}(x, y)| \quad (5)$$

Note that these scores sometimes do not agree with each other. For example, Fig. 5 shows a comparison of two models over **ECSSD** using PR and ROC metrics. While there is not a big difference in ROC curves (thus about the same AUC), one model clearly scores better using the PR curve (thus having higher F_β). Such disparity between the ROC and PR measures has been extensively studied in [107]. Note that the number of negative examples (non-salient pixels) is typically much bigger than the number of positive examples (salient object pixels) in evaluating salient object detection models. Therefore, PR curves are more informative than ROC curves and can present an over optimistic view of an algorithm's performance [107]. Thus we mainly base our conclusions on the PR curves scores (*i.e.*, F-Measure scores), and also report other scores for comprehensive comparisons and for facilitating specific application requirements. It is worth mentioning that active research is ongoing to figure out the better ways of measuring salient object detection and segmentation models (*e.g.* [108]).

D. Quantitative Comparison of Models

We evaluate saliency maps produced by different models on six datasets by using all evaluation metrics:

- 1) Fig. 6 and Fig. 7 show PR and ROC curves;
- 2) Fig. 8 and Fig. 9 demonstrate AUC and MAE scores;
- 3) Fig. 10 shows the F_β scores of all models².

In terms of both **PR** and **ROC** curves, DRFI model surprisingly outperforms all other models on six benchmark datasets with large margins. Besides, RBD, DSR and MC (solid lines with blue, yellow, and magenta colors, respectively) achieve close performance and perform slightly better than other models.

Using the **F-measure** (*i.e.*, F_β), the five best models are: DRFI, MC, RBD, DSR, and GMR, where DRFI model consistently wins over all the 5 datasets. MC ranks the second best over 2 datasets and the third best over 2 datasets. SR and SIM models perform the worst.

With respect to the **AUC** score, DRFI again ranks the best over all six datasets. Following DRFI, DSR model ranks the second over 4 datasets. RBD ranks the second on 1 dataset and the third on 2 datasets. While PCA ranks the third on 1 dataset in terms of AUC score, it is not on the list of top three contenders using F_β measure. IT, LC, and SR achieve the worst performance. It is worth being mentioned that all the models perform well above chance level (AUC = 0.5) on six benchmark datasets.

²Three segmentation methods are used, including adaptive threshold, fixed threshold, and SaliencyCut algorithm. The influence of segmentation methods will be discussed in Sect. III-A

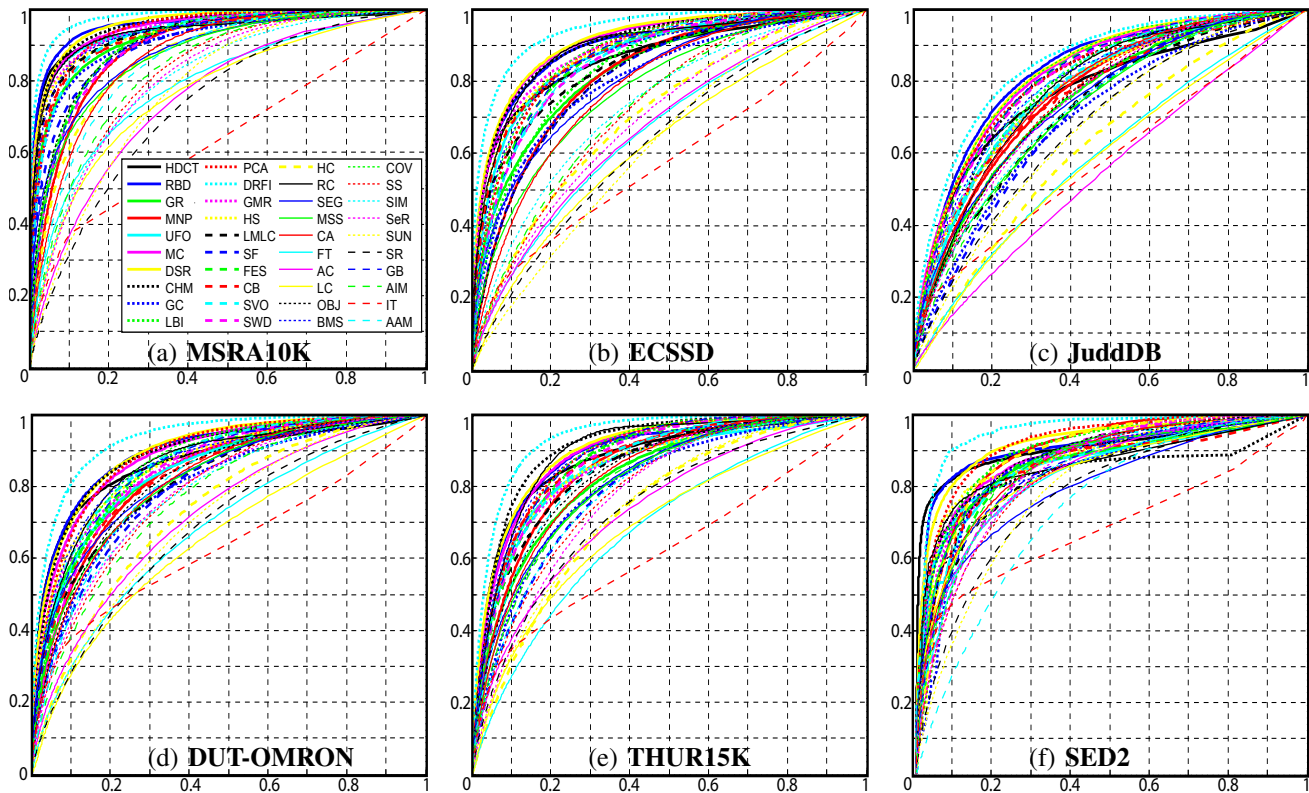


Fig. 7. ROC curves of models on 6 benchmarks. False and true positive rates are shown in x and y axes, respectively.

Rankings of models using MAE are more diverse than either F_β or AUC scores. DSR, RBD and DRFI rank on the top, but none of them are among top three models over **JuddDB**. MC, which performs well in terms of F_β and AUC, is not included in the top three models on any dataset. PCA performs the best on **JuddDB** but worse on others. SIM and SVO models perform the worst.

On average, the compared fixation prediction and object proposal generation models perform worse than salient object detection models. As two outliers, COV and BMS outperform several salient object detection models in terms of all evaluation metrics, implying that they are suitable for detecting salient proto objects. Additionally, Fig. 11 shows the distribution of F_β , ROC and MAE scores of all salient object detection models versus all fixation prediction models over all benchmark datasets. We can see a sharp separation of models especially for the F_β score, where most of the top models are salient object detection models. This result is consistent with the conclusion in [1] that fixation prediction models perform lower than salient object detection models. Though stemming from fixation prediction, research in salient object detection shares its unique properties and has truly added to what traditional saliency models focusing on fixation prediction already offer.

In particular, most of the 28 salient object detection models outperform the baseline AAM model. Among these 28 models, AAM only outperforms 2 models over **MSRA10K**, 8 over **ECSSD**, 4 on **THUR15K**, 12 on **JuddDB**, and 4 on **DUT-OMRON** in terms of F_β . Interestingly, AAM model does not outperform any model over **SED2**, which means

that indeed there is less center bias in this dataset and salient object detection models can detect off-center objects. Notice that AAM ranks lowest on **SED2** compared to other datasets. Please notice that it does not necessarily mean that models below AAM are not good, as taking advantage of the location prior may further enhance their performance (e.g., LC and FT).

On average, over all models and scores, the performances were lower on **JuddDB**, **DUT-OMRON** and **THUR15K**, implying that these datasets were more challenging. The low model performance of **JuddDB** can be caused by both less center bias and small objects in images. Noisy labeling of **DUT-OMRON** dataset might also be a reason for low model performance. By investigating some images of these two datasets for which models performed low, we found that there are several objects that can be potentially the most salient one. This makes the generation of ground-truth quite subjective and challenging, although the most salient object in **JuddDB** has objectively been defined to be the most looked-at one measured from eye movement data.

E. Qualitative Comparison of Models

Fig. 12 shows output maps of all models for a sample image with relatively complex background. Dark blue areas are less salient while dark red indicates higher saliency values. Compared with other models, top contenders like DRFI and DSR suppress most of the background well while almost successfully detect the whole salient object. They thus generate higher precision scores and less false

Model	THUR15K	JuddDB	DUT-OMRON	SED2	MSRA10K	ECSSD
HDCT	.878	.771	.869	.898	.941	.866
RBD	.887	.826	.894	.899	.955	.894
GR	.829	.747	.846	.854	.925	.831
MNP	.854	.768	.835	.888	.895	.820
UFO	.853	.775	.839	.845	.938	.875
MC	.895	.823	.887	.877	.951	.910
DSR	.902	.826	.899	.915	.959	.914
CHM	.910	.797	.890	.831	.952	.903
GC	.803	.702	.796	.846	.912	.805
LBI	.876	.792	.854	.896	.910	.842
PCA	.885	.804	.887	.911	.941	.876
DRFI	.938	.851	.933	.944	.978	.944
GMR	.856	.781	.853	.862	.944	.889
HS	.853	.775	.860	.858	.933	.883
LMLC	.853	.724	.817	.826	.936	.849
SF	.799	.711	.803	.871	.905	.817
FES	.867	.805	.848	.838	.898	.860
CB	.870	.760	.831	.839	.927	.875
SVO	.865	.784	.866	.875	.930	.857
SWD	.873	.812	.843	.845	.901	.857
HC	.735	.626	.733	.880	.867	.704
RC	.896	.775	.859	.852	.936	.892
SEG	.818	.747	.825	.796	.882	.808
MSS	.813	.726	.817	.871	.875	.779
CA	.830	.774	.815	.853	.872	.784
FT	.684	.593	.682	.820	.790	.661
AC	.740	.548	.721	.831	.756	.668
LC	.696	.586	.654	.827	.771	.627
OBJ	.839	.750	.822	.870	.907	.818
BMS	.879	.788	.856	.852	.929	.865
COV	.883	.826	.864	.833	.904	.879
SS	.792	.754	.784	.826	.823	.725
SIM	.797	.727	.783	.833	.808	.734
SeR	.778	.746	.786	.835	.813	.695
SUN	.746	.674	.708	.789	.778	.623
SR	.741	.676	.688	.769	.736	.633
GB	.882	.815	.857	.839	.902	.865
AIM	.814	.719	.768	.846	.833	.730
IT	.623	.586	.636	.682	.640	.577
AAM	.849	.797	.814	.736	.857	.863

Fig. 8. AUC: area under ROC curve (Higher is better. The top three models are highlighted in red, green and blue).

positive rates. Some models that include a center-bias component also result in appealing maps, *e.g.*, CB. Interestingly, region-based approaches, *e.g.*, RC, HS, DRFI, BMR, CB, and DSR always preserve the object boundary well compared with other pixel-based or patch-based models.

We can also clearly see the distinctness of different categories of models. Salient object detection models try to highlight the whole salient object and suppress the background. Fixation prediction models often produce blob-like and sparse saliency maps corresponding to the fixation areas of humans on scenes. The objectness map is a rough indication of the salient object. The output of the latter two types of models might not suit to segment the whole salient object well.

Model	THUR15K	JuddDB	DUT-OMRON	SED2	MSRA10K	ECSSD
HDCT	.177	.209	.164	.162	.143	.199
RBD	.150	.212	.144	.130	.108	.173
GR	.256	.311	.259	.189	.198	.285
MNP	.255	.286	.272	.215	.229	.307
UFO	.165	.216	.173	.180	.150	.207
MC	.184	.231	.186	.182	.145	.204
DSR	.142	.196	.139	.140	.121	.173
CHM	.153	.226	.152	.168	.142	.195
GC	.192	.258	.197	.185	.139	.214
LBI	.239	.273	.249	.207	.224	.280
PCA	.198	.181	.206	.200	.185	.248
DRFI	.150	.213	.155	.130	.118	.166
GMR	.181	.243	.189	.163	.126	.189
HS	.218	.282	.227	.157	.149	.228
LMLC	.246	.303	.277	.269	.163	.260
SF	.184	.218	.183	.180	.175	.230
FES	.155	.184	.156	.196	.185	.215
CB	.227	.287	.257	.195	.178	.241
SVO	.382	.422	.409	.348	.331	.404
SWD	.288	.292	.310	.296	.267	.318
HC	.291	.348	.310	.193	.215	.331
RC	.168	.270	.189	.148	.137	.187
SEG	.336	.354	.337	.312	.298	.342
MSS	.178	.204	.177	.192	.203	.245
CA	.248	.282	.254	.229	.237	.310
FT	.241	.267	.250	.206	.235	.291
AC	.186	.239	.190	.206	.227	.265
LC	.229	.277	.246	.204	.233	.296
OBJ	.306	.359	.323	.269	.262	.337
BMS	.181	.233	.175	.184	.151	.216
COV	.155	.182	.156	.210	.197	.217
SS	.267	.301	.277	.266	.266	.344
SIM	.414	.412	.429	.384	.388	.433
SeR	.345	.379	.352	.290	.310	.404
SUN	.310	.319	.349	.307	.306	.396
SR	.175	.200	.181	.220	.232	.266
GB	.229	.261	.240	.242	.222	.263
AIM	.298	.331	.322	.262	.286	.339
IT	.199	.200	.198	.245	.213	.273
AAM	.248	.343	.288	.405	.260	.276

Fig. 9. MAE: Mean Absolute Error (Smaller is better. The top three models are highlighted in red, green and blue).

III. PERFORMANCE ANALYSIS

Based on the performances reported above, we also conduct several experiments to provide a detailed analysis of all the benchmarking models and datasets.

A. Analysis of Segmentation Methods

In many computer vision and graphics applications, segmenting regions of interest is of great practical importance [36], [44], [47]–[49], [109], [110]. The simplest way of segmenting a salient object is to binarize the saliency map using a fixed threshold, which might be hard to choose. In this section, we extensively evaluate two additional most commonly used salient object segmentation methods, including adaptive threshold [18] and SaliencyCut [68].

Model	THUR15K			JuddDB			DUT-OMRON			SED2			MSRA10K			ECSSD		
	Fixed	AdpT	SCut	Fixed	AdpT	SCut	Fixed	AdpT	SCut	Fixed	AdpT	SCut	Fixed	AdpT	SCut	Fixed	AdpT	SCut
HDCT	.602	.571	.636	.412	.378	.422	.609	.572	.643	.822	.802	.758	.837	.807	.877	.705	.669	.740
RBD	.596	.566	.618	.457	.403	.461	.630	.580	.647	.837	.825	.750	.856	.821	.884	.718	.680	.757
GR	.551	.509	.546	.418	.338	.378	.599	.540	.580	.798	.753	.639	.816	.770	.830	.664	.583	.677
MNP	.495	.523	.603	.367	.337	.405	.467	.486	.576	.621	.778	.765	.668	.724	.822	.568	.555	.709
UFO	.579	.557	.610	.432	.385	.433	.545	.541	.593	.742	.781	.729	.842	.806	.862	.701	.654	.739
MC	.610	.603	.600	.460	.420	.434	.627	.603	.615	.779	.803	.630	.847	.824	.855	.742	.704	.745
DSR	.611	.604	.597	.454	.421	.410	.626	.614	.593	.794	.821	.632	.835	.824	.833	.737	.717	.703
CHM	.612	.591	.643	.417	.368	.424	.604	.586	.637	.750	.750	.658	.825	.804	.857	.722	.684	.735
GC	.533	.517	.497	.384	.321	.342	.535	.528	.506	.729	.730	.616	.794	.777	.780	.641	.612	.593
LBI	.519	.534	.618	.371	.353	.416	.482	.504	.609	.692	.776	.764	.696	.714	.857	.586	.563	.738
PCA	.544	.558	.601	.432	.404	.368	.554	.554	.624	.754	.796	.701	.782	.782	.845	.646	.627	.720
DRFI	.670	.607	.674	.475	.419	.447	.665	.605	.669	.831	.839	.702	.881	.838	.905	.787	.733	.801
GMR	.597	.594	.579	.454	.409	.432	.610	.591	.591	.773	.789	.643	.847	.825	.839	.740	.712	.736
HS	.585	.549	.602	.442	.358	.428	.616	.565	.616	.811	.776	.713	.845	.800	.870	.731	.659	.769
LMLC	.540	.519	.588	.375	.302	.397	.521	.493	.551	.653	.712	.674	.801	.772	.860	.659	.600	.735
SF	.500	.495	.342	.373	.319	.219	.519	.512	.377	.764	.794	.509	.779	.759	.573	.619	.576	.378
FES	.547	.575	.426	.424	.411	.333	.520	.555	.380	.617	.785	.174	.717	.753	.534	.645	.655	.467
CB	.581	.556	.615	.444	.375	.435	.542	.534	.593	.730	.704	.657	.815	.775	.857	.717	.656	.761
SVO	.554	.441	.609	.414	.279	.419	.557	.407	.609	.744	.667	.746	.789	.585	.863	.639	.357	.737
SWD	.528	.560	.649	.434	.386	.454	.478	.506	.613	.548	.714	.737	.689	.705	.871	.624	.549	.781
HC	.386	.401	.436	.286	.257	.280	.382	.380	.435	.736	.759	.646	.677	.663	.740	.460	.441	.499
RC	.610	.586	.639	.431	.370	.425	.599	.578	.621	.774	.807	.649	.844	.820	.875	.741	.701	.776
SEG	.500	.425	.580	.376	.268	.393	.516	.450	.562	.704	.640	.669	.697	.585	.812	.568	.408	.715
MSS	.478	.490	.200	.341	.324	.089	.476	.490	.193	.743	.783	.298	.696	.711	.362	.530	.536	.203
CA	.458	.494	.557	.353	.330	.394	.435	.458	.532	.591	.737	.565	.621	.679	.748	.515	.494	.625
FT	.386	.400	.238	.278	.250	.132	.381	.388	.259	.715	.734	.436	.635	.628	.472	.434	.431	.257
AC	.410	.431	.068	.227	.199	.049	.354	.383	.040	.684	.729	.140	.520	.566	.014	.411	.410	.038
LC	.386	.408	.289	.264	.246	.156	.327	.353	.243	.683	.752	.486	.569	.589	.432	.390	.396	.219
OBJ	.498	.482	.593	.368	.282	.413	.481	.445	.578	.685	.723	.731	.718	.681	.840	.574	.456	.698
BMS	.568	.578	.594	.434	.404	.416	.573	.576	.580	.713	.760	.627	.805	.798	.822	.683	.659	.690
COV	.510	.587	.398	.429	.427	.315	.486	.579	.373	.518	.724	.212	.667	.755	.394	.641	.677	.413
SS	.415	.482	.523	.344	.321	.397	.396	.443	.502	.533	.696	.641	.572	.642	.675	.467	.441	.574
SIM	.372	.429	.568	.295	.292	.384	.358	.402	.539	.498	.685	.725	.498	.585	.794	.433	.391	.672
SeR	.374	.419	.536	.316	.285	.388	.385	.411	.532	.521	.714	.702	.542	.607	.755	.419	.391	.596
SUN	.387	.432	.486	.303	.291	.285	.321	.360	.445	.504	.661	.613	.505	.596	.670	.388	.376	.478
SR	.374	.457	.002	.279	.270	.001	.298	.363	.000	.504	.700	.002	.473	.569	.001	.381	.385	.001
GB	.526	.571	.650	.419	.396	.455	.507	.548	.638	.571	.746	.695	.688	.737	.837	.624	.613	.765
AIM	.427	.461	.559	.317	.260	.360	.361	.377	.495	.541	.718	.693	.555	.575	.750	.449	.357	.571
IT	.373	.437	.005	.297	.283	.000	.378	.449	.005	.579	.697	.008	.471	.586	.158	.407	.414	.003
AAM	.458	.569	.620	.392	.367	.411	.406	.514	.534	.388	.524	.640	.580	.692	.779	.597	.627	.756

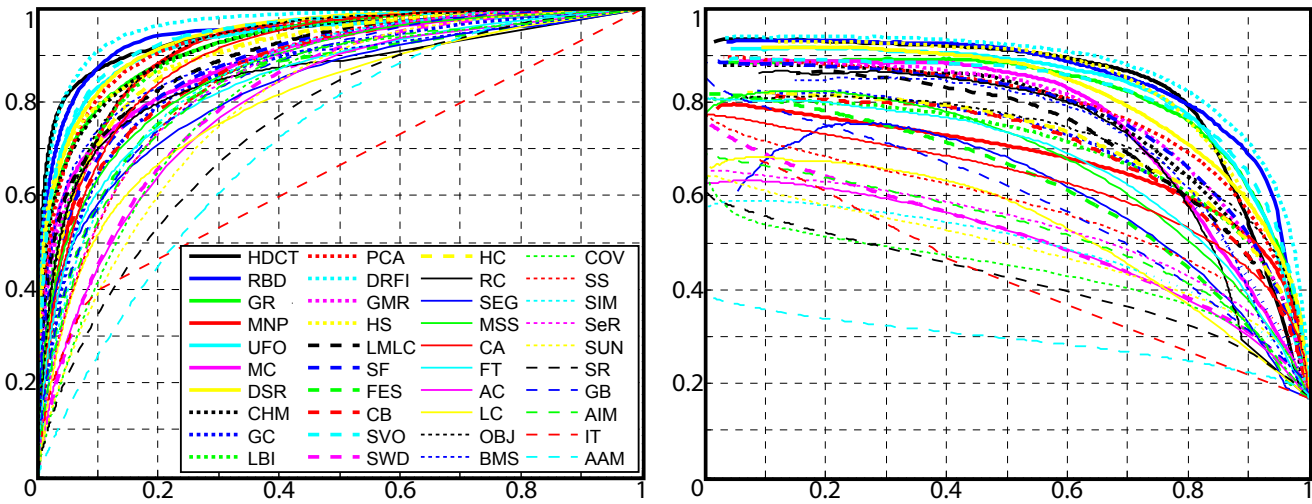
Fig. 10. F_β statistics on each dataset, using varying fixed thresholds, adaptive threshold, and SaliencyCut (Higher is better. The top three models are highlighted in red, green and blue).

Average F_β scores for salient object segmentation results on six benchmark datasets are shown in Fig. 10. Each segmentation algorithm was fed with saliency maps produced by all 40 compared models.

Except **JuddDB** and **SED2** datasets, best segmentation results are all achieved via SaliencyCut method combined with a sophisticated salient object detection model (e.g., DRFI, RBD, MNP). This suggests that enforcing label consistency in terms of using graph-based segmentation and global appearance statistics benefits salient object segmentations. The default SaliencyCut [68] program only outputs the most dominate salient object, This causes results for **SED2** and **JuddDB** benchmarks to be less optimal, as images in these two datasets (see Fig. 3) do not follow the

“single none ambiguous salient object assumption” made in [68].

As also observed by most works in image segmentation literature, nearby pixels with similar appearance tend to have similar object labels. To validate this, we demonstrated in Fig. 13(a) some better segmentation results by further enforcing label consistency among nearby and similar pixels. Enforcing such label consistency often helps improve labeling pixels specially when the majority of the salient object pixels have been highlighted in the detection phase. Challenging examples might still exist, however, such as complex object topology, spindle components, and similar appearance with respect to image background. More results of using the best combination, DRFI saliency maps and



Method	HDCT	RBD	GR	MNP	UFO	MC	DSR	CHM	GC	LBI	PCA	DRFI	GMR	HS	LMLC	SF	FES	CB	SVO
Max	.822	.811	.791	.661	.805	.764	.776	.746	.697	.685	.750	.831	.754	.815	.720	.747	.621	.693	.792
AUC	.941	.943	.925	.912	.929	.888	.938	.920	.860	.910	.928	.964	.886	.918	.896	.885	.839	.872	.942
MAE	.122	.106	.183	.188	.128	.171	.117	.138	.164	.197	.162	.127	.148	.150	.201	.150	.160	.207	.325

Method	SWD	HC	RC	SEG	MSS	CA	FT	AC	LC	OBJ	BMS	COV	SS	SIM	SeR	SUN	SR	GB	AIM	IT	AAM
Max	.521	.700	.744	.629	.666	.620	.671	.521	.569	.708	.739	.463	.571	.515	.546	.498	.444	.590	.540	.460	.328
AUC	.813	.898	.855	.828	.868	.896	.843	.800	.797	.915	.879	.805	.852	.858	.849	.795	.750	.850	.836	.655	.716
MAE	.291	.176	.177	.300	.167	.199	.183	.177	.192	.243	.146	.176	.225	.363	.273	.276	.184	.208	.265	.165	.406

Fig. 15. Results of center-bias analysis over 1000 less center-biased images chosen from the **MSRA10K** dataset. Top: ROC and PR curves, Bottom: Mean F_β , AUC, and MAE scores for all models.

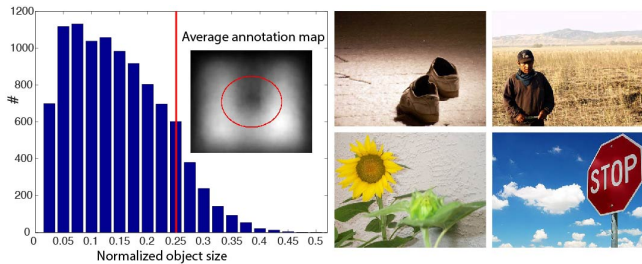


Fig. 14. Left: Histogram of object center over all images, threshold (red line = 0.247), and annotation map over 1000 less center-biased images in **MSRA10K** dataset. Right: Four less center-biased images. The overlaid circle illustrates the center-bias threshold.

are all shown in Fig. 15. DRFI and DSR again perform the best. Overall, most models’ performance decrease when testing on no/less center biased images (e.g., the AUC score of MC declines from 0.951 to 0.888), while a few others show increase. For example, the AUC score of SVO raises from 0.930 to 0.942 and it gets the second ranking. Some models, e.g., HS (with the second ranking in terms of F_β score), performs better according to their rank changes w.r.t the whole **MSRA10K** dataset. DRFI still wins over other models here with a large margin. The difference in F_β , AUC, and MAE scores are not very big for this model over all data and 1000 less center-biased images (difference are 0.05, 0.05, and 0.009, respectively). This means that this model is not taking advantage of center-bias much. In

the contrast, CB model uses a lot of location prior and that is why its performance drops heavily when applied to these images (difference are 0.122, 0.122, and 0.029, respectively).

Additionally, it can be observed from Fig. 2(f), there is less center bias over the **SED2** dataset where there is less activation in the center of its average annotation map. We can therefore study the center bias on it. Similarly, DRFI and DSR outperforms other models in terms of F_β , AUC, and MAE scores, indicating they are more robust to the location variations of salient objects. HS again ranks second according to the F_β score. Fig. 16 shows best and worst un-centered stimuli for DRFI and DSR models.

Overall, all the models perform well above the chance level over either the less center-biased subset of **MSRA10K** or **SED2**. It is also worth noticing that the AAM model performs significantly worse on these two datasets, as well as **JuddDB**, validating our motivation of studying center bias on them.

C. Analysis of Salient Object Existence

Almost all of existing salient object detection models assume that there is at least one salient object in the input image. This impractical assumption might lead to less optimal performance on “background images”, which do not contain any dominated salient objects, as studied in [111]. To verify the effectiveness of models on back-

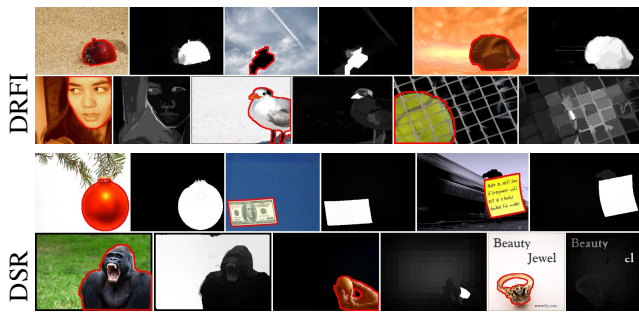


Fig. 16. Top and Bottom rows for each model illustrate best and worst cases in un-centered images.

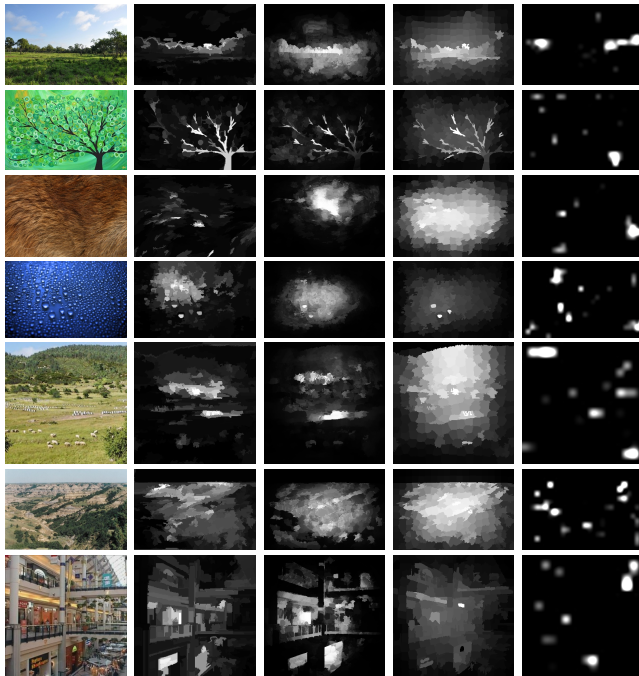


Fig. 17. Sample background-only images and prediction maps of DRFI, DSR, MC, and IT models.

ground images, we collected 800 images from the web and evaluated compared models on them.

We can see from Fig. 17 that there exist no dominated salient objects in background images that consist of only textures or cluttered background. A good model should generate a dark saliency map, *i.e.*, without any activation as there are no salient objects. For quantitative evaluation, we only report the MAE score of each model, which is basically the sum of non-zero elements of the output saliency map. Note that it is not feasible to calculate PR and ROC curves here since the ground truth positive labeling here is empty. Also notice that ground truth of eye fixations do exist on such background images.

Fig. 17 shows some sample background images and their output saliency maps using three top salient object detection models on a classical fixation prediction model. Fig. 18 reports MAE scores of 35 models. Top salient object detection models like DRFI, DSR, and MC do not perform well and often generate activations on the background images even though only regular textures exist (the third

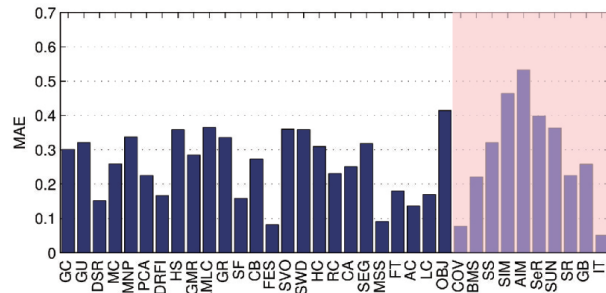


Fig. 18. MAE over background-only images with no salient objects. Shaded area belongs to fixation prediction models.

and fourth rows of Fig. 17). This is reasonable as they always assume there exist salient objects in the input image and will try their best to find some ones. On the other hand, they can be distracted by the clutter in the background since high contrast always exist on the cluttered region. Most of existing salient object detections compute saliency based on contrast values. These cluttered regions are thus more likely considered as salient.

From Fig. 18, we can see that fixation prediction models COV and IT perform the best on background images in terms of the MAE scores. Compared with maps with dense salient regions produced by salient object models, maps generated by fixation prediction models often include sparse activations. See Fig. 17 for the output of the IT model. The sum of non-zero elements of such sparse saliency maps are smaller and thus the performance of COV and IT are better.

D. Analysis of Worst and Best Cases for Top Models

To understand what are the challenges for existing salient object detection models, we illustrate three the best and worst cases for top models over all six benchmark datasets. The stimuli for 11 top models were sorted according to the F_β scores. We only give a demonstration of DRFI and MC models in Fig. 19 due to limited space. See our online challenge website for additional illustrations.

It can be noticed from Fig. 19 that models share the same easy and difficult stimuli. Both DRFI and MC perform substantially well on the cases where a dominated salient object exists in a relatively clean background. Since most existing salient object detection models do not utilize any high-level prior knowledge, they may fail when a complex scene has a cluttered background or when the salient object is *semantically* salient (*e.g.*, DRFI fails on images with faces in **MSRA10K**). Another reason causing poor saliency detection is object size. Both DRFI and MC models have difficulty in detecting small objects (See hard cases on **DUT-OMRON** and **JuddDB**).

Particularly, since saliency cues adopted by DRFI are mainly based on contrast, this model fails on scenes where salient objects share close appearance with the background (*e.g.*, the hard cases of **MSRA10K** and **ECSSD**). Another possible reason is related to the failure in segmenting the image. MC relies on the pseudo-background prior that the image border areas are background. That is why it fails on

scenes where the salient object touches the image border, *e.g.*, the gorilla image in **MSRA10K** dataset (4th row of the right column of Fig. 19).

E. Runtime Analysis

Runtime of 40 compared models are shown in Fig. 1 over all 10K images of **MSRA10K** (typical image resolution of 400×300) using an Intel Xeon E5645 2.40GHz CPU with 8 GB RAM. The LC model here is the fastest (about 0.009 seconds per image) followed by HC and GC models. The best model in our benchmark (DRFI) needs about 0.697 seconds to process one image.

IV. DISCUSSIONS AND CONCLUSIONS

From the results obtained so far, we summarize in Fig. 20 the rankings of models based on average performance over all 6 datasets in terms of segmentation methods, center bias, salient object existence, and run time³. Based on the rankings, we conclude that:

“DRFI, RBD, DSR, MC, HDCT, and HS are the top 6 models for salient object detection.”

By investigating the performances and the design choices of all compared models, our extensive evaluations do suggest some clear messages about commonly used design choices, which could be valuable for developing future algorithms. We refer readers to our recent survey [28] for a comprehensive review of different design choices adopted for salient object detection.

- From the elements perspective, all top six models are built upon superpixels (regions). On the one hand, compared with pixels, more effective features (*e.g.*, color histogram) can be extracted from regions. On the other hand, compared with patches, the boundary of the salient object is better preserved for region-based approaches, leading to more accurate detection performance. Moreover, since the number of pixels is far less than the number of pixels or patches, region-based methods has the potential to run faster.
- All the top six models explicitly consider the background prior, which assumes that that the area in the narrow border of the image belongs to the background. Compared with the location prior of a salient object, such a background prior performs more robust.
- The leading method in our benchmark (*i.e.*, DRFI), discriminatively trains a regression model to predict region saliency according to a 93-dimensional feature vector. Instead of purely relying on the cues extracted only from the input image, DRFI resorts to human annotations to automatically discover feature integration rules. The high performance of this simple learning-based method encourages pursuing data-driven approaches for salient object detection.

³We have created a unified repository for sharing code and data where researchers can run models with a single click or can add new models for benchmarking purposes. All codes, data, and results are available in our online benchmark website: <http://mmcheng.net/salobjbenchmark/>

Even considering top performing models, salient object detection still seems far from being solved. To achieve more appealing results, three challenges should be addressed. First, in our large-scale benchmark (see Sec. II), all top performing algorithms use the location prior cues, limiting their adaptation to general cases. Second, although the ranking of top scoring models are quite consistent across datasets, performance scores (F_β and AUC) drop significantly from easier datasets to more difficult ones. Third challenge regards the run time of models. Some models need around one minute to process a 400×300 image (*e.g.*, CA: 40.9s, SVO: 56.5s, and LMLC 140s).

One area for future research would be designing scores for tackling dataset biases and evaluation of saliency segmentation maps with respect to ground-truth annotations similar to [108]. In this benchmark, we only focused on single-input scenarios. Although some RGBD datasets exist [112], benchmark datasets for multiple input images (*e.g.*, salient object detection on videos, co-salient object detection [28]) are still lacking. Another future direction will be following active segmentation algorithms (*e.g.*, [99], [113], [114]) by segmenting a salient object from a seed point. Finally, aggregation of saliency models for building a strong prediction model (similar to [1], [115], and behavioral investigation of saliency judgments by humans (*e.g.*, [21], [116]) are two other interesting directions.

REFERENCES

- [1] A. Borji, D. N. Sihite, and L. Itti, “Salient object detection: A benchmark,” in *ECCV*, 2012, pp. 414–429.
- [2] A. Borji and L. Itti, “State-of-the-art in visual attention modeling,” *IEEE TPAMI*, vol. 35, no. 1, pp. 185–207, 2013.
- [3] A. Borji, D. Sihite, and L. Itti, “Quantitative analysis of human-model agreement in visual saliency modeling: A comparative study,” *IEEE TIP*, vol. 22, no. 1, pp. 55–69, 2013.
- [4] M. Hayhoe and D. Ballard, “Eye movements in natural behavior,” *Trends in cognitive sciences*, pp. 188–194, 2005.
- [5] L. Itti and C. Koch, “Computational modelling of visual attention,” *Nature reviews neuroscience*, vol. 2, no. 3, pp. 194–203, 2001.
- [6] A. M. Treisman and G. Gelade, “A feature-integration theory of attention,” *Cognitive Psychology*, pp. 97–136, 1980.
- [7] J. M. Wolfe, K. R. Cave, and S. L. Franzel, “Guided search: an alternative to the feature integration model for visual search,” *J. Exp. Psychol. Human*, vol. 15, no. 3, p. 419, 1989.
- [8] J. M. Wolfe, “Guidance of visual search by preattentive information,” in *Neurobiology of Attention*, 2005, pp. 101–104.
- [9] C. Koch and S. Ullman, “Shifts in selective visual attention: towards the underlying neural circuitry,” in *Matters of Intelligence*, 1987, pp. 115–141.
- [10] L. Itti, C. Koch, and E. Niebur, “A model of saliency-based visual attention for rapid scene analysis,” *IEEE TPAMI*, 1998.
- [11] D. Parkhurst, K. Law, and E. Niebur, “Modeling the role of saliency in the allocation of overt visual attention,” *Vision Research*, vol. 42, no. 1, pp. 107–123, 2002.
- [12] J. Li, Y. Tian, T. Huang, and W. Gao, “Probabilistic multi-task learning for visual saliency estimation in video,” *IJCV*, vol. 90, no. 2, pp. 150–165, Nov. 2010.
- [13] A. Borji and L. Itti, “Exploiting local and global patch rarities for saliency detection,” in *CVPR*, 2012, pp. 478–485.
- [14] A. Borji, “Boosting bottom-up and top-down visual features for saliency estimation,” in *CVPR*, 2012, pp. 438–445.
- [15] K. Koehler, F. Guo, S. Zhang, and M. P. Eckstein, “What do saliency models predict?” *J. Vision*, 2014.
- [16] J. Li, Y. Tian, and T. Huang, “Visual saliency with statistical priors,” *IJCV*, vol. 107, no. 3, pp. 239–253, 2014.
- [17] T. Liu, J. Sun, N. Zheng, X. Tang, and H.-Y. Shum, “Learning to detect a salient object,” in *CVPR*, 2007, pp. 1–8.

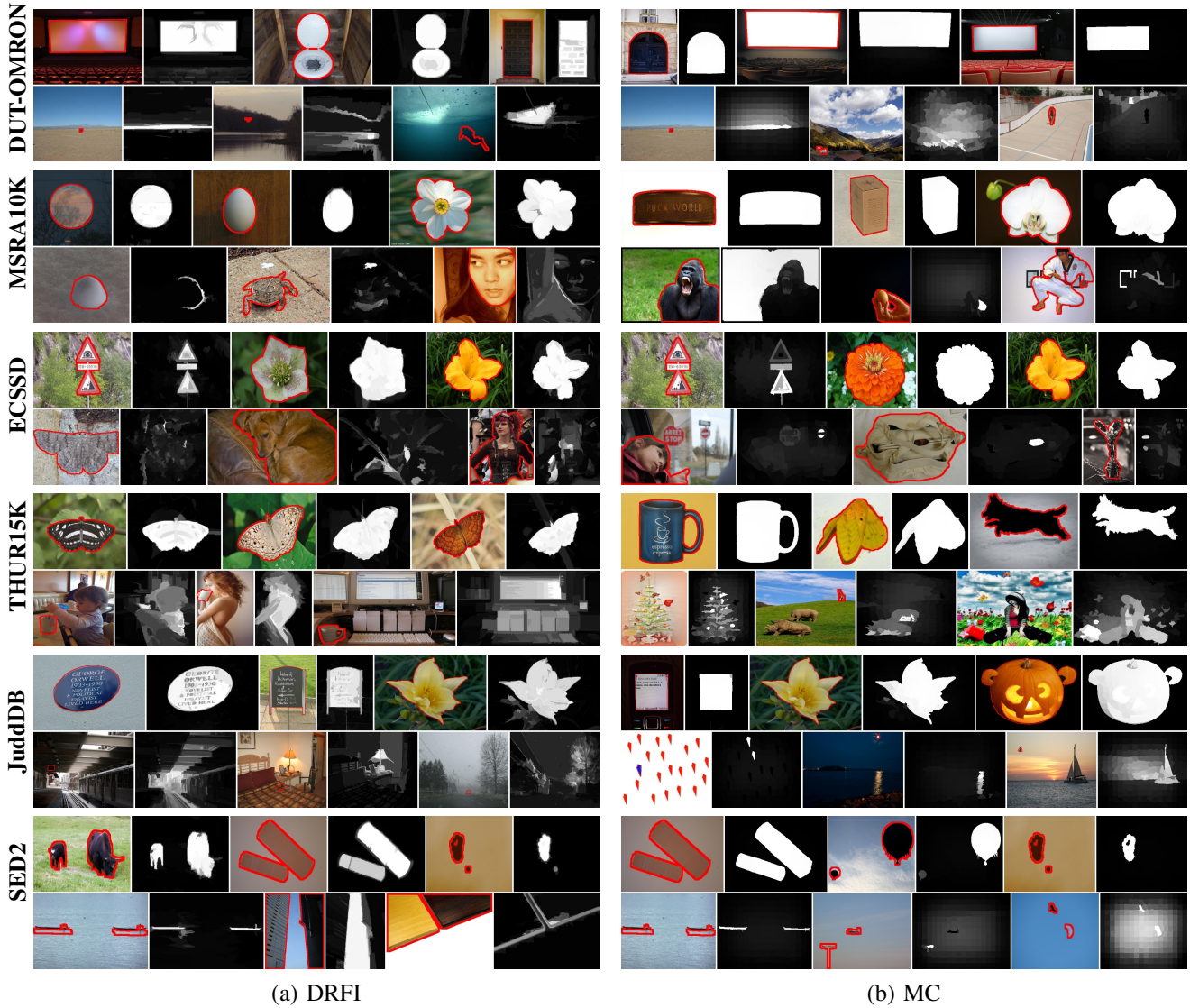


Fig. 19. Best (1st rows for each model on a dataset) and worst (2nd rows) cases of DRFI and MC. Ground-truth object(s) is denoted by a red contour.

Method	HDCT	RBD	GR	MNP	UFO	MC	DSR	CHM	GC	LBI	PCA	DRFI	GMR	HS	LMLC	SF	FES	CB	SVO
F_β	8	3	10	27	11	2	4	9	16	23	14	1	5	6	17	19	18	12	15
AUC	7	3	21	20	16	4	2	6	28	13	5	1	9	12	23	26	18	19	11
MAE	5	2	26	28	6	11	1	4	15	23	16	3	9	17	27	13	8	21	39
AdpT	7	5	17	21	13	3	2	8	19	20	12	1	4	14	25	18	11	16	37
SCut	4	2	24	14	8	13	20	11	29	9	15	1	17	7	18	33	32	12	10
CB	2	4	7	24	5	9	8	13	19	21	11	1	10	3	16	12	26	20	6
Time	27	15	23	34	33	13	30	32	13	39	28	19	11	17	38	14	8	24	37

Method	SWD	HC	RC	SEG	MSS	CA	FT	AC	LC	OBJ	BMS	COV	SS	SIM	SeR	SUN	SR	GB	AIM	IT	AAM
F_β	20	30	7	22	26	28	32	34	36	25	13	24	31	39	35	38	40	21	33	37	29
AUC	17	31	8	29	27	24	37	35	39	22	14	10	32	33	34	36	38	15	30	40	25
MAE	33	30	7	37	14	29	25	19	24	35	12	10	32	40	38	36	18	22	34	20	31
AdpT	22	29	6	36	24	26	32	35	33	27	9	10	28	34	31	39	40	15	38	30	23
SCut	3	30	6	22	37	27	35	38	36	16	21	34	28	23	25	31	40	5	26	39	19
CB	34	18	14	25	23	27	22	33	30	17	15	37	29	35	31	36	39	28	32	38	40
Time	12	2	10	31	7	36	6	9	1	25	18	35	5	21	22	26	4	20	29	16	40

Fig. 20. Summary rankings of models under different evaluation metrics. The first three rows show average ranking scores over all 6 datasets using best fixed thresholding, adaptive thresholding, and SaliencyCut. The fourth row shows results using best fixed thresholding over none-center biased images. Fixation prediction models are shown in bold face. The top three models under each evaluation metric are highlighted in red, green and blue.

- [18] R. Achanta, S. Hemami, F. Estrada, and S. Süsstrunk, "Frequency-tuned salient region detection," in *CVPR*, 2009.
- [19] Y. Tian, J. Li, S. Yu, and T. Huang, "Learning complementary saliency priors for foreground object segmentation in complex scenes," *IJCV*, 2014.
- [20] J. Wang, L. Quan, J. Sun, X. Tang, and H.-Y. Shum, "Picture collage," in *CVPR*, vol. 1, 2006, pp. 347–354.
- [21] A. Borji, D. N. Sihite, and L. Itti, "What stands out in a scene? a study of human explicit saliency judgment," *Vision Research*, vol. 91, no. 0, pp. 62–77, 2013.
- [22] U. Rutishauser, D. Walther, C. Koch, and P. Perona, "Is bottom-up attention useful for object recognition?" in *CVPR*, 2004.
- [23] C. Kanan and G. Cottrell, "Robust classification of objects, faces, and flowers using natural image statistics," in *CVPR*, 2010, pp. 2472–2479.
- [24] F. Moosmann, D. Larlus, and F. Jurie, "Learning saliency maps for object categorization," in *ECCV Workshop*, 2006.
- [25] A. Borji, M. N. Ahmadabadi, and B. N. Araabi, "Cost-sensitive learning of top-down modulation for attentional control," *Machine Vision and Applications*, 2011.
- [26] A. Borji and L. Itti, "Scene classification with a sparse set of salient regions," in *IEEE ICRA*, 2011, pp. 1902–1908.
- [27] H. Shen, S. Li, C. Zhu, H. Chang, and J. Zhang, "Moving object detection in aerial video based on spatiotemporal saliency," *Chinese Journal of Aeronautics*, 2013.
- [28] A. Borji, M.-M. Cheng, H. Jiang, and J. Li, "Salient object detection: A survey," *arXiv preprint arXiv:1411.5878*, 2014.
- [29] Z. Ren, S. Gao, L.-T. Chia, and I. Tsang, "Region-based saliency detection and its application in object recognition," *IEEE TCSVT*, vol. PP, no. 99, pp. 1–1, 2013.
- [30] C. Guo and L. Zhang, "A novel multiresolution spatiotemporal saliency detection model and its applications in image and video compression," *IEEE TIP*, 2010.
- [31] L. Itti, "Automatic foveation for video compression using a neurobiological model of visual attention," *IEEE TIP*, 2004.
- [32] Y.-F. Ma, X.-S. Hua, L. Lu, and H.-J. Zhang, "A generic framework of user attention model and its application in video summarization," *IEEE TMM*, 2005.
- [33] Y. J. Lee, J. Ghosh, and K. Grauman, "Discovering important people and objects for egocentric video summarization," in *CVPR*, 2012, pp. 1346–1353.
- [34] Q.-G. Ji, Z.-D. Fang, Z.-H. Xie, and Z.-M. Lu, "Video abstraction based on the visual attention model and online clustering," *Signal Processing: Image Communication*, 2012.
- [35] S. Goferman, A. Tal, and L. Zelnik-Manor, "Puzzle-like collage," *Computer Graphics Forum*, 2010.
- [36] H. Huang, L. Zhang, and H.-C. Zhang, "Arcimboldo-like collage using internet images," *ACM Transactions on Graphics*, vol. 30, no. 6, p. 155, 2011.
- [37] A. Ninassi, O. Le Meur, P. Le Callet, and D. Barba, "Does where you gaze on an image affect your perception of quality? applying visual attention to image quality metric," in *IEEE ICIP*, vol. 2, 2007, pp. II–169.
- [38] H. Liu and I. Heynderickx, "Studying the added value of visual attention in objective image quality metrics based on eye movement data," in *IEEE ICIP*, 2009, pp. 3097–3100.
- [39] A. Li, X. She, and Q. Sun, "Color image quality assessment combining saliency and fsm," in *ICDIP*, vol. 8878, 2013.
- [40] M. Donoser, M. Urschler, M. Hirzer, and H. Bischof, "Saliency driven total variation segmentation," in *ICCV*, 2009.
- [41] Q. Li, Y. Zhou, and J. Yang, "Saliency based image segmentation," in *ICMT*, 2011, pp. 5068–5071.
- [42] C. Qin, G. Zhang, Y. Zhou, W. Tao, and Z. Cao, "Integration of the saliency-based seed extraction and random walks for image segmentation," *Neurocomputing*, vol. 129, 2013.
- [43] M. Johnson-Roberson, J. Bohg, M. Bjorkman, and D. Kragic, "Attention-based active 3d point cloud segmentation," in *IEEE IROS*, 2010, pp. 1165–1170.
- [44] T. Chen, M.-M. Cheng, P. Tan, A. Shamir, and S.-M. Hu, "Sketch2photo: internet image montage," *ACM TOG*, 2009.
- [45] S. Feng, D. Xu, and X. Yang, "Attention-driven salient edge (s) and region (s) extraction with application to CBIR," *Signal Processing*, vol. 90, no. 1, pp. 1–15, 2010.
- [46] J. Sun, J. Xie, J. Liu, and T. Sikora, "Image adaptation and dynamic browsing based on two-layer saliency combination," *IEEE Trans. Broadcasting*, vol. 59, no. 4, pp. 602–613, 2013.
- [47] L. Li, S. Jiang, Z. Zha, Z. Wu, and Q. Huang, "Partial-duplicate image retrieval via saliency-guided visually matching," *IEEE MultiMedia*, vol. 20, no. 3, pp. 13–23, 2013.
- [48] A. Y.-S. Chia, S. Zhuo, R. K. Gupta, Y.-W. Tai, S.-Y. Cho, P. Tan, and S. Lin, "Semantic colorization with internet images," *ACM TOG*, vol. 30, no. 6, p. 156, 2011.
- [49] H. Liu, L. Zhang, and H. Huang, "Web-image driven best views of 3d shapes," *The Visual Computer*, 2012.
- [50] R. Margolin, L. Zelnik-Manor, and A. Tal, "Saliency for image manipulation," *The Visual Computer*, pp. 1–12, 2013.
- [51] C. Goldberg, T. Chen, F.-L. Zhang, A. Shamir, and S.-M. Hu, "Data-driven object manipulation in images," *Computer Graphics Forum*, vol. 31, pp. 265–274, 2012.
- [52] S. Stalder, H. Grabner, and L. Van Gool, "Dynamic objectness for adaptive tracking," in *ACCV*, 2012.
- [53] J. Li, M. Levine, X. An, X. Xu, and H. He, "Visual saliency based on scale-space analysis in the frequency domain," *IEEE TPAMI*, vol. 35, no. 4, pp. 996–1010, 2013.
- [54] G. M. García, D. A. Klein, J. Stückler, S. Frintrop, and A. B. Cremers, "Adaptive multi-cue 3d tracking of arbitrary objects," in *Pattern Recognition*, 2012, pp. 357–366.
- [55] A. Borji, S. Frintrop, D. N. Sihite, and L. Itti, "Adaptive object tracking by learning background context," in *CVPR*, 2012.
- [56] D. A. Klein, D. Schulz, S. Frintrop, and A. B. Cremers, "Adaptive real-time video-tracking for arbitrary objects," in *IEEE IROS*, 2010, pp. 772–777.
- [57] S. Frintrop and M. Kessel, "Most salient region tracking," in *IEEE ICRA*, 2009, pp. 1869–1874.
- [58] G. Zhang, Z. Yuan, N. Zheng, X. Sheng, and T. Liu, "Visual saliency based object tracking," in *ACCV*, 2010.
- [59] A. Karpathy, S. Miller, and L. Fei-Fei, "Object discovery in 3d scenes via shape analysis," in *ICRA*, 2013, pp. 2088–2095.
- [60] S. Frintrop, G. M. Garcia, and A. B. Cremers, "A cognitive approach for object discovery," in *ICPR*, 2014.
- [61] D. Meger, P.-E. Forssén, K. Lai, S. Helmer, S. McCann, T. Southey, M. Baumann, J. J. Little, and D. G. Lowe, "Curious george: An attentive semantic robot," *Robotics and Autonomous Systems*, vol. 56, no. 6, pp. 503–511, 2008.
- [62] Y. Sugano, Y. Matsushita, and Y. Sato, "Calibration-free gaze sensing using saliency maps," in *CVPR*, 2010.
- [63] Y. Zhai and M. Shah, "Visual attention detection in video sequences using spatiotemporal cues," in *ACM Multimedia*, 2006, pp. 815–824.
- [64] R. Achanta, F. Estrada, P. Wils, and S. Süsstrunk, "Salient region detection and segmentation," in *Comp. Vis. Sys.*, 2008.
- [65] S. Goferman, L. Zelnik-Manor, and A. Tal, "Context-aware saliency detection," *IEEE TPAMI*, vol. 34, no. 10, 2012.
- [66] R. Achanta and S. Süsstrunk, "Saliency detection using maximum symmetric surround," in *Proceedings of the International Conference on Image Processing, ICIP 2010, September 26-29, Hong Kong, China*, 2010, pp. 2653–2656.
- [67] E. Rahtu, J. Kannala, M. Salo, and J. Heikkilä, "Segmenting salient objects from images and videos," in *ECCV*, 2010.
- [68] M.-M. Cheng, N. J. Mitra, X. Huang, P. H. S. Torr, and S.-M. Hu, "Global contrast based salient region detection," *IEEE TPAMI (CVPR 2011)*, 2014.
- [69] L. Duan, C. Wu, J. Miao, L. Qing, and Y. Fu, "Visual saliency detection by spatially weighted dissimilarity," in *CVPR*, 2011, pp. 473–480.
- [70] K.-Y. Chang, T.-L. Liu, H.-T. Chen, and S.-H. Lai, "Fusing generic objectness and visual saliency for salient object detection," in *ICCV*, 2011, pp. 914–921.
- [71] H. Jiang, J. Wang, Z. Yuan, T. Liu, and N. Zheng, "Automatic salient object segmentation based on context and shape prior," in *BMVC*, 2011.
- [72] H. R. Tavakoli, E. Rahtu, and J. Heikkilä, "Fast and efficient saliency detection using sparse sampling and kernel density estimation," in *Image Analysis - 17th Scandinavian Conference, SCIA 2011, Ystad, Sweden, May 2011. Proceedings*, 2011, pp. 666–675.
- [73] F. Perazzi, P. Krahenbuhl, Y. Pritch, and A. Hornung, "Saliency filters: Contrast based filtering for salient region detection," in *CVPR*, 2012, pp. 733–740.
- [74] Y. Xie, H. Lu, and M.-H. Yang, "Bayesian saliency via low and mid level cues," *IEEE TIP*, vol. 22, no. 5, 2013.
- [75] Q. Yan, L. Xu, J. Shi, and J. Jia, "Hierarchical saliency detection," in *CVPR*. CVPR, 2013, pp. 1155–1162.

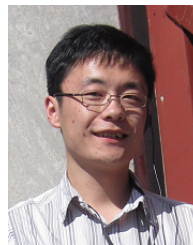
- [76] C. Yang, L. Zhang, H. Lu, X. Ruan, and M.-H. Yang, "Saliency detection via graph-based manifold ranking," in *CVPR*, 2013.
- [77] H. Jiang, J. Wang, Z. Yuan, Y. Wu, N. Zheng, and S. Li, "Salient object detection: A discriminative regional feature integration approach," in *IEEE CVPR*, 2013, pp. 2083–2090.
- [78] R. Margolin, A. Tal, and L. Zelnik-Manor, "What makes a patch distinct?" in *CVPR*, 2013, pp. 1139–1146.
- [79] P. Siva, C. Russell, T. Xiang, and L. Agapito, "Looking beyond the image: Unsupervised learning for object saliency and detection," in *CVPR*, 2013, pp. 3238–3245.
- [80] M.-M. Cheng, J. Warrell, W.-Y. Lin, S. Zheng, V. Vineet, and N. Crook, "Efficient salient region detection with soft image abstraction," in *ICCV*, 2013, pp. 1529–1536.
- [81] X. Li, Y. Li, C. Shen, A. R. Dick, and A. van den Hengel, "Contextual hypergraph modeling for salient object detection," in *ICCV*, 2013, pp. 3328–3335.
- [82] X. Li, H. Lu, L. Zhang, X. Ruan, and M.-H. Yang, "Saliency detection via dense and sparse reconstruction," in *ICCV*, 2013.
- [83] B. Jiang, L. Zhang, H. Lu, C. Yang, and M.-H. Yang, "Saliency detection via absorbing markov chain," in *ICCV*, 2013.
- [84] P. Jiang, H. Ling, J. Yu, and J. Peng, "Salient region detection by ufo: Uniqueness, focusness and objectness," in *ICCV*, 2013.
- [85] C. Yang, L. Zhang, and H. Lu, "Graph-regularized saliency detection with convex-hull-based center prior," *IEEE Signal Processing Letters*, vol. 20, no. 7, pp. 637–640, 2013.
- [86] W. Zhu, S. Liang, Y. Wei, and J. Sun, "Saliency optimization from robust background detection," in *CVPR*, 2014.
- [87] J. Kim, D. Han, Y.-W. Tai, and J. Kim, "Salient region detection via high-dimensional color transform," in *CVPR*, 2014.
- [88] N. D. Bruce and J. K. Tsotsos, "Saliency based on information maximization," in *NIPS*, 2005, pp. 155–162.
- [89] J. Harel, C. Koch, and P. Perona, "Graph-based visual saliency," in *NIPS*, 2007, pp. 545–552.
- [90] X. Hou and L. Zhang, "Saliency detection: A spectral residual approach," in *CVPR*, 2007, pp. 1–8.
- [91] L. Zhang, M. H. Tong, T. K. Marks, H. Shan, and G. W. Cottrell, "Sun: A bayesian framework for saliency using natural statistics," *J. Vision*, vol. 8, no. 7, pp. 32, 1–20, 2008.
- [92] H. J. Seo and P. Milanfar, "Static and space-time visual saliency detection by self-reseemblance," *J. Vision*, 2009.
- [93] N. Murray, M. Vanrell, X. Otazu, and C. A. Parraga, "Saliency estimation using a non-parametric low-level vision model," in *CVPR*, 2011, pp. 433–440.
- [94] X. Hou, J. Harel, and C. Koch, "Image signature: Highlighting sparse salient regions," *IEEE TPAMI*, vol. 34, no. 1, 2012.
- [95] E. Erdem and A. Erdem, "Visual saliency estimation by nonlinearly integrating features using region covariances," *J. Vision*, vol. 13, no. 4, pp. 11, 1–20, 2013.
- [96] J. Zhang and S. Sclaroff, "Saliency detection: A boolean map approach," in *ICCV*, 2013, pp. 153–160.
- [97] B. Alexe, T. Deselaers, and V. Ferrari, "What is an object?" in *CVPR*, 2010, pp. 73–80.
- [98] THUR15000, "http://mmcheng.net/gsal/."
- [99] A. Borji, "What is a salient object? a dataset and a baseline model for salient object detection," in *IEEE TIP*, 2014.
- [100] S. Alpert, M. Galun, R. Basri, and A. Brandt, "Image segmentation by probabilistic bottom-up aggregation and cue integration," in *CVPR*, 2007, pp. 1–8.
- [101] P. F. Felzenszwalb and D. P. Huttenlocher, "Efficient graph-based image segmentation," *IJCV*, pp. 167–181, 2004.
- [102] V. Movahedi and J. H. Elder, "Design and perceptual validation of performance measures for salient object segmentation," in *IEEE CVPRW*, 2010.
- [103] C. Rother, V. Kolmogorov, and A. Blake, "'GrabCut': interactive foreground extraction using iterated graph cuts," *ACM TOG*, vol. 23, no. 3, pp. 309–314, 2004.
- [104] T. Liu, Z. Yuan, J. Sun, J. Wang, N. Zheng, X. Tang, and H.-Y. Shum, "Learning to detect a salient object," *IEEE TPAMI*, vol. 33, no. 2, pp. 353–367, 2011.
- [105] D. R. Martin, C. C. Fowlkes, and J. Malik, "Learning to detect natural image boundaries using local brightness, color, and texture cues," *IEEE TPAMI*, vol. 26, no. 5, pp. 530–549, 2004.
- [106] S. Avidan and A. Shamir, "Seam carving for content-aware image resizing," in *ACM TOG*, vol. 26, no. 3, 2007, p. 10.
- [107] J. Davis and M. Goadrich, "The relationship between precision-recall and roc curves," in *ICML*, 2006, pp. 233–240.
- [108] R. Margolin, L. Zelnik-Manor, and A. Tal, "How to evaluate foreground maps?" in *CVPR*, 2014.
- [109] J.-Y. Zhu, J. Wu, Y. Wei, E. Chang, and Z. Tu, "Unsupervised object class discovery via saliency-guided multiple class learning," in *CVPR*, 2012, pp. 3218–3225.
- [110] J. He, J. Feng, X. Liu, T. Cheng, T.-H. Lin, H. Chung, and S.-F. Chang, "Mobile product search with bag of hash bits and boundary reranking," in *Computer Vision and Pattern Recognition (CVPR), 2012 IEEE Conference on*. IEEE, 2012, pp. 3005–3012.
- [111] P. Wang, J. Wang, G. Zeng, J. Feng, H. Zha, and S. Li, "Salient object detection for searched web images via global saliency," in *CVPR*, 2012, pp. 3194–3201.
- [112] H. Peng, B. Li, W. Xiong, W. Hu, and R. Ji, "Rgb salient object detection: a benchmark and algorithms," in *ECCV*, 2014, pp. 92–109.
- [113] A. K. Mishra, Y. Aloimonos, L. F. Cheong, and A. Kassim, "Active visual segmentation," *IEEE TPAMI*, vol. 34, 2012.
- [114] Y. Li, X. Hou, C. Koch, J. M. Rehg, and A. L. Yuille, "The secrets of salient object segmentation," in *CVPR*, 2014.
- [115] L. Mai, Y. Niu, and F. Liu, "Saliency aggregation: A data-driven approach," in *CVPR*, 2013, pp. 1131–1138.
- [116] A. Borji, D. N. Sihite, and L. Itti, "Objects do not predict fixations better than early saliency: A re-analysis of einhäuser et al.'s data," *J. Vision*, vol. 13, no. 10, p. 18, 2013.



Ali Borji received his BS and MS degrees in computer engineering from Petroleum University of Technology, Tehran, Iran, 2001 and Shiraz University, Shiraz, Iran, 2004, respectively. He did his Ph.D. in cognitive neurosciences at Institute for Studies in Fundamental Sciences (IPM) in Tehran, Iran, 2009 and spent four years as a postdoctoral scholar at iLab, University of Southern California from 2010 to 2014. He is currently an assistant professor at University of Wisconsin, Milwaukee. His research interests include visual attention, active learning, object and scene recognition, and cognitive and computational neurosciences.



Ming-Ming Cheng received his PhD degree from Tsinghua University in 2012. He is currently a research fellow in Oxford University, working with Prof. Philip Torr. His research interests include computer graphics, computer vision, image processing, and image retrieval. He has received the Google PhD fellowship award, the IBM PhD fellowship award, and the new PhD Researcher Award from Chinese Ministry of Education.



Huaizu Jiang is currently working as a research assistant at Institute of Artificial Intelligence and Robotics, Xi'an Jiaotong University. Before that, he received his BS and MS degrees from Xi'an Jiaotong University, China, in 2005 and 2009, respectively. He is interested in how to teach an intelligent machine to understand the visual scene like a human. Specifically, his research interests include object detection, large-scale visual recognition, and (3D) scene understanding.



Jia Li received his B.E. degree from Tsinghua University in 2005 and Ph.D. degree from the Chinese Academy of Sciences in 2011. During 2011 and 2013, he used to serve as a research fellow and visiting assistant professor in Nanyang Technological University, Singapore. He is currently an associate professor at Beihang University, Beijing, China. His research interests include visual attention/saliency modeling, multimedia analysis, and vision from Big Data.